

CO₂ Uptake and Cyclic Stability of MgO-Based CO₂ Sorbents Promoted with Alkali Metal Nitrates and Their Eutectic Mixtures

Journal Article

Author(s):

Dal Pozzo, Alessandro; [Armutlulu, Andac](#) ; Rekhtina, Margarita; Abdala, Paula M.; Müller, Christoph R.

Publication date:

2019-02-25

Permanent link:

<https://doi.org/https://doi.org/10.3929/ethz-b-000327318>

Rights / license:

[In Copyright - Non-Commercial Use Permitted](#)

Originally published in:

ACS Applied Energy Materials 2(2), <https://doi.org/10.1021/acsaem.8b01852>

Funding acknowledgement:

- Next generation CaO-based CO₂ sorbents: X-ray absorption spectroscopy and advanced electron microscopy techniques ()

CO₂ Uptake and Cyclic Stability of MgO-Based CO₂ Sorbents Promoted with Alkali Metal Nitrates and Their Eutectic Mixtures

Alessandro Dal Pozzo ^{a,b}, Andaç Armutlulu ^b, Margarita Rekhtina ^b, Paula M. Abdala, Christoph R. Müller ^{b,*}

^a Laboratory of Industrial Safety and Environmental Sustainability
Department of Civil, Chemical, Environmental and Materials Engineering, Alma Mater Studiorum - Università di Bologna, via Terracini 28, 40131 Bologna, Italy

^b Laboratory of Energy Science and Engineering
Department of Mechanical and Process Engineering, ETH Zürich, Leonhardstrasse 21, 8092 Zürich, Switzerland

*Corresponding author. Tel.: +41 44 632 3440.
E-mail address: muelchri@ethz.ch (Prof. Christoph Müller)

ABSTRACT

CO₂ capture and storage (CCS) is a technological solution to stabilize or even reduce the atmospheric concentration of the greenhouse gas CO₂, to mitigate climate change. In this context, MgO is a promising solid CO₂ sorbent, as the energy penalty sorbent regeneration is comparatively small, but it requires the addition of promoters, typically alkali metal nitrates, to yield acceptable kinetics. Under operating conditions, the promoters are in a molten state. The main objectives of this work are (i) to assess experimentally the validity of different reaction mechanisms for the CO₂ uptake of promoted MgO that are currently debated in literature and (ii) to elucidate the processes that lead to sorbent deactivation. Our experimental results support the mechanism in which the dissolution of MgO in the molten nitrate promoter is the rate-limiting step for carbonation. We were able to establish a direct correlation between the solubility of MgO in the promoter and the initial rate of carbonation. In addition, a systematic study of a large number of promoter compositions (mixtures of LiNO₃, NaNO₃, KNO₃) indicate that promoters with a lower melting point exhibit higher CO₂ uptakes, presumably due to their lower viscosity and, thus, higher ion mobility at a given temperature. Concerning the cyclic stability of promoted MgO, a decay of its CO₂ uptake with number of carbonation/calcination cycles is ascribed only partially to sintering. Instead, the surface migration of the promoter was identified as an at least equally relevant deactivation mechanism. Importantly, it was also found that the CO₂ uptake of the deactivated sorbent can be restored to a large extent with a simple hydration step.

Keywords: CO₂ capture, molten salts, alkali metal nitrate, MgO, deactivation, cyclic stability

1 INTRODUCTION

The atmospheric concentration of carbon dioxide (CO₂) has increased by more than 45 % with respect to pre-industrial levels, highlighting that anthropogenic emissions of CO₂ are most likely the main contributors to global warming ^{1,2}. Since the worldwide consumption of fossil fuels still increases year by year, coal, oil and natural gas are expected to maintain their major role in the global energy mix in the near- to mid-term future ³. Therefore, the deployment of industrial CO₂ capture and storage (CCS) technologies will be critical to achieve an appreciable reduction of anthropogenic CO₂ emissions in the near term ⁴.

Among the different technologies proposed for CCS, the use of solid sorbents is receiving increasing attention, owing to their low cost and relatively high sorption capacity ⁵⁻⁷. In particular, alkaline earth metal oxides can capture CO₂ through the carbonation reaction and are regenerated via the reverse, i.e. calcination reaction, typically performed by a temperature swing. The feasibility of such a cyclic operation has already been tested in a number of pilot plants, using limestone-derived CaO as the CO₂ sorbent ⁸. However, pure CaO suffers from a poor cyclic stability owing to a sintering-induced capacity decay ⁹. Despite recent efforts to improve the cyclic stability of CaO-based sorbents ^{10,11}, the full-scale implementation of CaO-based CCS is still associated with a high energy penalty due to the high temperature for sorbent regeneration ¹².

This has triggered a resurgence of research aiming at using magnesium oxide (MgO) as a CO₂ sorbent. When compared to CaO ¹³, MgO offers (i) a higher theoretical CO₂ uptake capacity of ~1.09 g CO₂/g MgO and (ii) operation in a low- to moderate temperature range (i.e., 200 – 450 °C), and thus a reduced energy penalty for sorbent regeneration when compared to e.g., CaO, Li₂ZrO₃ ¹⁴ and Li₄SiO₄ ¹⁵. The underlying CO₂ capture reaction of MgO is its carbonation, viz.



Regeneration (i.e., the release of a pure stream of CO₂) is typically performed via a temperature swing (calcination reaction) which requires temperatures exceeding 400 °C to yield a stream of pure CO₂ ¹⁶.

However, in spite of its high theoretical capture capacity, the actual CO₂ uptake of pure MgO is significantly lower, i.e., < 4 wt. %. This has been attributed to the rapid formation of a dense MgCO₃ layer on its surface, hindering the further carbonation of unreacted MgO through mass transfer limitations ^{17,18}. Therefore, the primary focus of previous research efforts has been the development of approaches to reduce the limitations due to product layer formation. For example, Zarghami *et al.* ¹⁶ found that increasing the system pressure to 20 bar and adding 30 vol. % water vapor improved the apparent rate of carbonation, leading in turn to an almost complete conversion of the solid sorbent. Ding *et al.* ¹⁹ showed that even at atmospheric pressure MgO can indeed reach CO₂ uptakes that are four times higher than for the reference dry gas when exposed to 70 % relative humidity. Yet, the recorded CO₂ uptakes were still far from the maximal theoretical CO₂ uptake capacity of MgO. The improved kinetics in the presence of steam was attributed to an adsorbed layer of water which may promote the formation of Mg²⁺ ions ¹⁸.

More recently, the addition of alkali metal nitrates (e.g., LiNO₃, NaNO₃, KNO₃) to MgO has been found to increase appreciably its CO₂ uptake capacity. Vu *et al.* ²⁰ reported that MgO-KNO₃ composites yielded a CO₂ uptake of 13.9 wt. % for a carbonation time of 2 h at 325 °C. Zhang *et al.* ²¹ and Prashar *et al.* ²² obtained NaNO₃-promoted MgO by ball milling or impregnation and reported a CO₂ uptake as high as 57.6 wt. % after 1 h of carbonation at 330 °C. Harada *et al.* ²³ showed that

MgO coated with a ternary mixture of Li, Na, K nitrates yielded a CO₂ uptake of 43.6 wt. % for a carbonation time of 4 h at 300 °C. In addition, the material showed a satisfactory regenerability and faster carbonation kinetics compared to MgO mixed with a single nitrate. It is worth noting that the promoting effect of NaNO₃ was also reported for dolomite²⁴, Na-Mg double salts²⁵ and synthetic hydrotalcite²⁶. The most recent works that aimed at improving the mixing between the promoter and MgO reported CO₂ uptakes as high as 0.7-0.8 g CO₂/g sorbent²⁷⁻³¹.

Although it has been established that the addition of alkali metal nitrates improves appreciably the CO₂ uptake of MgO, the mechanism through which alkali metal nitrates promote the CO₂ uptake is currently not completely understood and different hypotheses have been put forward^{21,23}. Given the typical reaction temperatures for the carbonation of MgO (viz. 250 – 350 °C), it can be assumed that the promoters are in a molten state.

Harada *et al.*²³ and other researchers^{20,32,33} have argued that the molten layer of nitrates acts primarily as a diffusion medium for CO₂, allowing for an improved contact between MgO and the gaseous reactant. While carbonation on bare MgO produces a rigid, monodentate carbonate layer impermeable for gaseous reactants, in nitrate-promoted MgO the molten layer dissolves CO₂ and, owing to the high concentration of oxygen (O²⁻) ions in the nitrate melt, carbonate (CO₃²⁻) ions form rapidly²³ leading in turn to the fast formation of MgCO₃. On the other hand, Zhang *et al.*²¹ and other investigators^{34,35} have hypothesized that the main role of the molten nitrates is to dissolve bulk MgO, thus overcoming its high lattice energy barrier for carbonation. The dissolution of MgO leads to [Mg²⁺ ... O²⁻] ionic pairs. The CO₂ adsorbed on bare MgO can migrate to the gas-liquid-solid interface and react with the solvated ionic pairs in the melt to form [Mg²⁺ ... CO₃²⁻] pairs, which eventually, upon saturation, precipitate as solid MgCO₃. In the first reaction model the carbonation of MgO is controlled by the solubility of CO₂ in the nitrates, while in the second reaction scheme the dissolution of MgO in the promoter melt is the rate controlling step. Elucidation of the validity of the two reaction schemes proposed is a critical step to develop more effective MgO-based CO₂ sorbents³⁶.

Besides the reaction mechanism, it is currently also unclear which properties of the promoters control the CO₂ uptake. Although it has been established that the promoter has to be in a molten state to be effective, differences in the CO₂ uptake between a number of promoters have not been explained yet²⁹. Hence, a systematic study of a large variety of promoters (and mixtures thereof) at identical testing conditions is of interest to the community as it would allow the identification of the promoter properties that are most relevant for the optimization of the CO₂ uptake of MgO. Such a systematic study is reported here.

Another concern related to promoted MgO-based CO₂ sorbents is their deactivation with number of carbonation and calcination cycles. Indeed, deactivation in the range of 30-60% of the initial uptake has been reported^{23,33,34}. Previous studies have attributed the decay in the CO₂ uptake of MgO largely to sintering, however without providing experimental evidence^{23,27,28}, assuming instead an analogy to the behavior of CaO-based sorbents^{10,11,37,38}. Only recently, Zhao *et al.*³¹ provided evidence that the surface area and pore size of a NaNO₃-promoted mesoporous MgO sorbent decreased after carbonation and subsequent regeneration. However, recent work indicates that the loss of CO₂ carrying capacity might not only be related to changes in the morphology of the material (i.e. pore volume and surface area), but also due to some partial de-wetting of the MgO surface³⁹. Observing a different contact angle of NaNO₃ drops on MgO and MgCO₃ surfaces, Jo *et al.*³⁹ argued that the “repulsive” carbonate surface might lead to a migration of NaNO₃ upon carbonation. As a consequence, after regeneration, the surface of calcined MgO would have a poorer coverage with NaNO₃, leading to a lower active surface area and hence, a smaller CO₂ uptake. Yet, so far there is

no experimental support for the deactivation mechanism proposed by Jo *et al.* ³⁹. Elucidation of the prevailing deactivation mechanism is important to devise countermeasures to re-activate a sorbent.

Considering the uncertainties concerning the reaction and deactivation mechanisms of promoted MgO-based CO₂ sorbents, the systematic assessment of a large number of promoters and mixtures thereof reported here, allowed us to narrow down further on the prevailing reaction and deactivation mechanisms of this class of CO₂ sorbents. Using our improved understanding of the deactivation mechanism, an inexpensive re-activation route is reported. The new insights reported here provide the basis for the fabrication of more effective, yet inexpensive MgO-based CO₂ sorbents.

2 EXPERIMENTAL

Synthesis. Alkali metal nitrate-promoted MgO was prepared via the wet mixing of commercial basic magnesium carbonate ($\text{Mg}_5(\text{CO}_3)_4(\text{OH})_2 \cdot 4\text{H}_2\text{O}$, Acros Organics), also known as hydromagnesite (HM), with alkali metal salts and the subsequent calcination of the slurries obtained. Alkali metal nitrates (LiNO_3 , NaNO_3 , KNO_3) were purchased from Sigma-Aldrich. In a typical synthesis, 6 g of MgO precursor (corresponding to ~ 0.07 mol of Mg) and appropriate amounts of salts (5-70 % molar ratio with respect to Mg) were mixed in 15 mL of deionized (DI) water and stirred magnetically for 1 h at room temperature. **Table 1** summarizes the compositions of the synthesized samples.

The aqueous slurries were dried in an oven at 120 °C overnight, ground with a mortar and placed in a muffle furnace for calcination in air (450 °C, 4 h, heating rate 3 °C/ min). The selected calcination temperature allowed for a calcination of both MgCO_3 and $\text{Mg}(\text{OH})_2$ without causing a significant decomposition of the alkali metal nitrate mixtures (expected to occur at temperatures exceeding 550 °C) ⁴⁰.

Table 1: Summary of the composition and melting points of the salt mixture of the promoted MgO samples.

Salt mixture	Composition (molar fraction in the mixture)			Melting point of the salt mixture (°C) ^a
	LiNO ₃	NaNO ₃	KNO ₃	
LiNO ₃	1	-	-	255
NaNO ₃	-	1	-	308
KNO ₃	-	-	1	334
(Li,K)NO ₃	0.9	-	0.1	240
	0.7	-	0.7	200
	0.45	-	0.55	130 ^b
	0.3	-	0.7	200
	0.1	-	0.9	300
(Na,K)NO ₃	-	0.9	0.1	290
	-	0.8	0.2	270
	-	0.6	0.4	230
	-	0.46	0.54	221 ^b
	-	0.4	0.6	230
	-	0.25	0.75	270
(Li,Na)NO ₃	0.8	0.2	-	230
	0.6	0.4	-	200
	0.5	0.5	-	200 ^b
	0.4	0.6	-	220
	0.2	0.8	-	270
(Li,Na,K)NO ₃	0.3	0.5	0.2	215
	0.3	0.18	0.52	120 ^b
	0.3	0.1	0.6	160

a: Experimentally determined melting point of the mixture of alkali metal nitrates⁴¹.

b: Eutectic point of the binary or ternary mixtures^{42,43}.

In control experiments, MgO was replaced by CaO or aluminum oxide (Al₂O₃), while alkali metal carbonates (Li₂CO₃, Na₂CO₃, K₂CO₃), silver nitrate (AgNO₃) and chlorides (LiCl, KCl) were assessed as alternative promoters. In addition to HM, the following MgO precursors were also used: commercial magnesium hydroxide (Mg(OH)₂, Sigma-Aldrich) and laboratory-synthesized magnesium carbonate (MgCO₃). The latter was prepared by the precipitation of a 1 M solution of magnesium nitrate (Mg(NO₃)₂, Sigma-Aldrich) with a 2 M solution of sodium carbonate (Na₂CO₃, Sigma-Aldrich). During precipitation the pH value was kept constant (pH = 11) through the dropwise addition of a 3 M solution of sodium hydroxide (NaOH, Fisher Chemicals). The performance of the MgO-based sorbents that have been derived from other precursors than commercial HM are reported in **Fig. S1** of the Supporting Information (SI).

Performance characterization. The CO₂ uptake of the sorbents was measured in a thermogravimetric analyzer (TGA, Mettler Toledo TGA/DSC 3+). A small amount (~10 mg) of the sorbent was placed in an alumina crucible and pre-calcined at 450 °C under a N₂ flow of 80 mL/min for 30 min to remove adsorbed water and ensure that the sorbent was in the calcined state. Subsequently, the sample was cooled down to the desired reaction temperature and the gas flow was switched to CO₂ (80 mL/min). Repeated cycles of carbonation and regeneration were performed at

the desired reaction temperature in 100% CO₂ for 1 h and regeneration at 450 °C in 100% N₂ for 15 min. The reaction conditions were chosen in accordance to previous reports, allowing for a comparison between the different studies ²¹⁻²³. To assess the effect of steam on the CO₂ uptake characteristics, the gas flow was bubbled through a saturator (located outside of the reaction chamber) filled with de-ionized water. The steam concentration in the TGA at 300 °C was ~2.0 vol %.

XRD measurements. The crystalline phases present in the sorbents were investigated using X-ray powder diffraction (Bruker, AXS D8 Advance) using Cu K α radiation with a wavelength of 1.5406 Å. The X-ray diffractometer was operated at 40 mA and 40 kV. Each sample was scanned within the 2 θ range of 10–90°. The step size was 0.025° with a time duration per step of 0.8 s.

The mean size τ of the crystallites was estimated using the Scherrer equation:

$$\tau = \frac{K\lambda}{\Delta_{1/2}\cos\theta}$$

where K , λ , $\Delta_{1/2}$, and θ are the shape factor (0.94 for spherical particles), the X-ray wavelength, the peak width at half the maximum intensity and the reflection angle, respectively. Rietveld refinement of the XRD data was performed using the FullProf suite ⁴⁴.

DRIFTS spectra. Diffuse reflectance infrared spectroscopy (Nicolet, 6700 FT-IR) was employed to characterize the carbonates formed. *In situ* DRIFTS data were collected by placing the sample in a Harrick Praying Mantis cell. After heating up to 450 °C in N₂, the sample was exposed to a CO₂ flow of 30 mL/min at different temperatures (100, 150, 200, 250, 275, 300, 350, 400 °C).

Solubility experiments. The dissolution of MgO in different alkali metal nitrates was studied by immersing a single crystal of pure MgO (Sigma Aldrich) in a crucible filled with nitrate powder. The mole ratio of MgO to alkali metal nitrate was maintained in each run. The dissolution of MgO took place at 350 °C in a N₂ atmosphere for 10 h. The amount of Mg retained in the cooled nitrate melt was quantified by inductively coupled plasma-optical emission spectrometry (ICP-OES).

3 RESULTS & DISCUSSION

3.1 Characterization of synthesized sorbents

Fig. 1 shows SEM images and XRD patterns of a representative sample in which the HM (hydromagnesite, Mg₅(CO₃)₄(OH)₂·4H₂O) precursor was promoted by 10 mol % NaNO₃. The as-prepared sample, (i.e. dried after the wet mixing of HM with NaNO₃), exhibits a plate-like morphology that is indeed typical for HM ⁴⁵. Upon calcination, MgO with an average particle diameter of < 100 nm was obtained (**Fig. 1b**). Rietveld refinement of the XRD pattern of MgO - 10 mol % NaNO₃ (**Fig. S2**) confirms that the phase composition of the material synthesized is close to the expected values. The grain-like morphology of the sample is maintained after exposure to a CO₂ atmosphere at 300 °C (**Fig. 1c-d**) leading to the partial conversion of MgO to MgCO₃, as confirmed by XRD (**Fig. 1e**). After 10 carbonation and calcination cycles (carbonated state), the peaks due to MgCO₃ appear less intense (relative intensities with respect to MgO peaks) compared to the first cycle and, most likely due to a decreasing CO₂ uptake with cycle number.

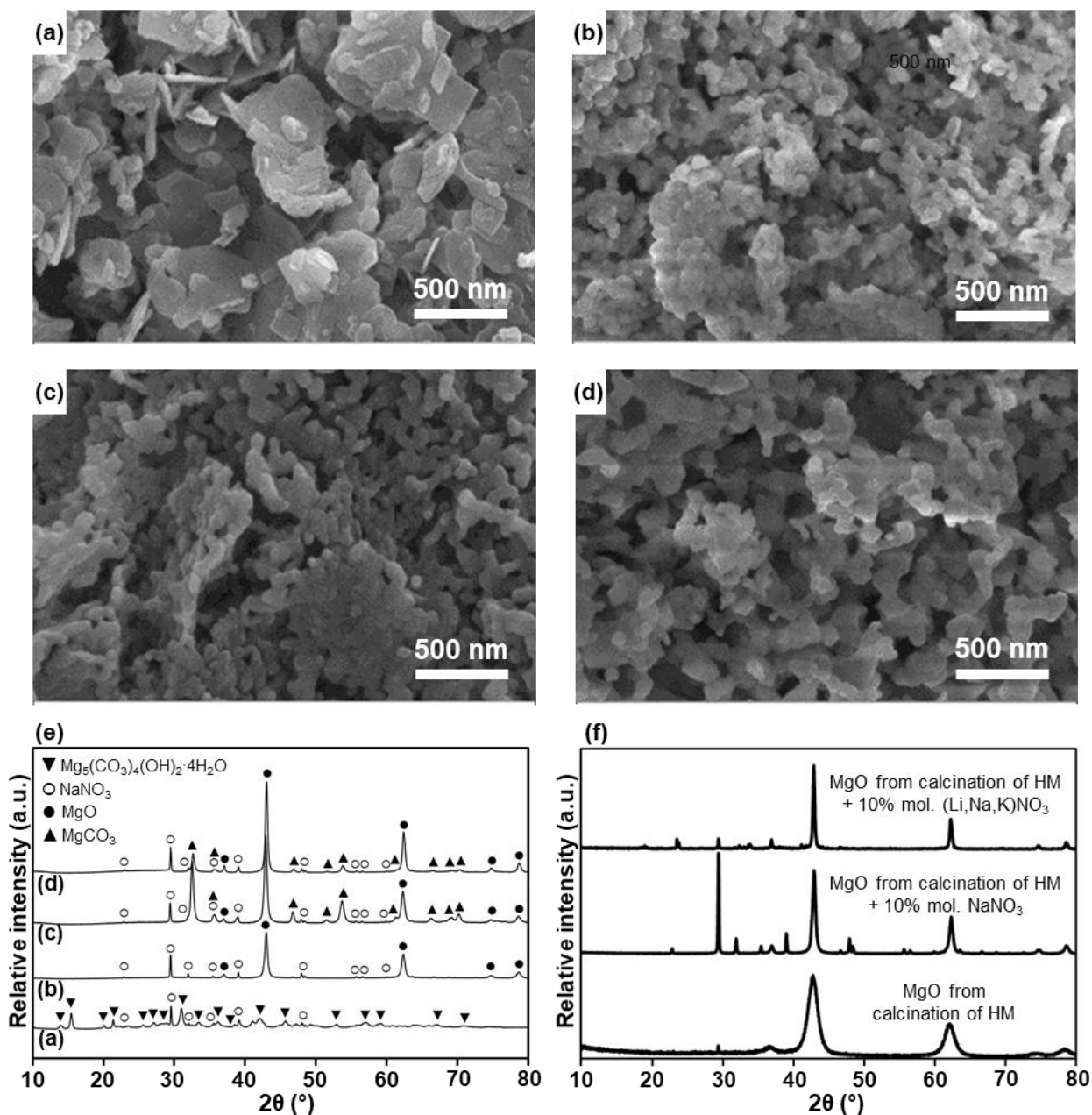


Fig. 1: SEM images of MgO - 10 mol % NaNO₃: **a)** after drying (as prepared), **b)** after calcination at 450 °C (calcined), **c)** after 1 h of carbonation at 300 °C in CO₂ (carbonated, 1 cycle), **d)** after 10 cycles of 1 h of carbonation at 300 °C and regeneration at 450 °C (carbonated, 10 cycles), Scale bars: 500 nm. **e)** XRD patterns of the samples shown in **(a-d)** and the identified phases at room temperature, **f)** XRD patterns of MgO obtained from the calcination of pure HM, HM with NaNO₃, and HM with (Li,Na,K)NO₃.

The XRD pattern of MgO promoted by NaNO₃ was compared to that of MgO obtained by the calcination of pure HM under the same conditions without the addition of nitrates (**Fig. 1f**). MgO peaks are considerably sharper in the sample calcined in the presence of NaNO₃, indicating that the presence of alkali metal nitrates affects the average crystallite size of MgO. The average crystallite size of the MgO obtained through the calcination of pure HM is 7-8 nm, while for MgO obtained through the calcination of HM in the presence of NaNO₃ or a ternary nitrate mixture (i.e., (Li,Na,K)NO₃) is noticeably larger (~20 nm). This suggests that the alkali metal nitrates accelerate

the crystal growth of MgO. In addition, monitoring the calcination of HM in a TGA (**Fig. S3**), it was observed that its promotion with NaNO₃ lowers the onset temperature of MgO formation when compared to the unpromoted sample. Specifically, the temperature for MgO formation (identified as the peak temperature of the associated weight loss event) is lowered by approximately 40, 55, and 75 °C in the presence of 2, 5, and 10 mol % NaNO₃, respectively. The coarser morphology of NaNO₃- or (Li,Na,K)NO₃-promoted MgO translates into a significantly lower surface area of, respectively, 27 m²/g and 22 m²/g, compared to 284 m²/g for MgO obtained through the calcination of HM.

3.2 Alkali metal (Li, Na, K) nitrate promotion on the CO₂ uptake of MgO

3.2.1 Temperature-programmed carbonation of unpromoted and promoted MgO

Fig. 2a plots the temperature-programmed carbonation (followed by TGA) of a series of alkali metal nitrate-promoted MgO sorbents. The samples were exposed to CO₂ while heating from 50 to 500 °C. Unpromoted MgO showed an immediate CO₂ uptake at the very beginning of the experiment (i.e., 50 °C), reaching its maximal CO₂ uptake at 150 °C and then slowly releasing the CO₂ absorbed with increasing temperature. The broad CO₂ desorption peak can be attributed to different (surface) species formed during the carbonation of unpromoted MgO, ranging from weakly physisorbed CO₂ to chemisorbed monodentate carbonates ^{46,47}.

Conversely, for MgO samples promoted with alkali metal nitrates, the extent of carbonation was negligible at low temperatures and accelerated abruptly after a threshold temperature was reached. This threshold temperature, determined as the inflection point of the CO₂ uptake curve (see **Fig. S4**), differed appreciably with the type of promoter used and appears to be linked to the physical state of the promoter. At low temperatures, the nitrates are in the solid state, hindering the carbonation of MgO by covering its surface with a solid film. When approaching the melting point of the alkali metal nitrate, the kinetics of CO₂ absorption increased dramatically. For MgO-LiNO₃ (MP_{LiNO₃} = 255 °C), the transition took place at 225 °C, whereas for MgO-NaNO₃ (MP_{NaNO₃} = 308 °C), the transition occurred at 275 °C owing to its higher melting point. The observation that the enhanced CO₂ absorption started at temperatures below the bulk melting temperature of the promoter can be explained by the fact that close to the melting point, the surface of the promoter is already partially disordered, leading to the partial formation of a liquid-like film at the interfaces (a phenomenon known as “premelting” ^{48,49}). For example, NaNO₃ undergoes a solid-state transition from an ordered to a disordered rhombohedral structure at 275 °C (33 °C below the melting point) ⁵⁰ and this structural rearrangement might trigger premelting, which in turn can be related to the observed simultaneous acceleration of CO₂ uptake.

Indeed, the onset temperature for the carbonation of MgO could be reduced further by its promotion with eutectic mixtures of alkali metal nitrates ⁵¹. **Fig. 2a** shows that, by lowering the melting point of the promoter through the use of a (Na,K)NO₃ eutectic mixture (60% NaNO₃, 40% KNO₃; MP = 230 °C), the onset temperature of carbonation is reduced to 230 °C. Using a ternary eutectic mixture (Li,Na,K)NO₃, MP = 120 °C), the onset temperature of carbonation is reduced further to 160 °C. The difference between the melting point of this promoting mixture and the onset temperature of (significant) carbonation in the temperature-programmed experiment suggests that at low temperatures the accelerating effect of the addition of alkali metal nitrates on the carbonation of MgO is reduced. When the carbonation time is extended to 10 h, the promoting effect of (Li,Na,K)NO₃ compared to unpromoted MgO is also visible at lower temperatures, i.e. near the melting point of the promoter (see **Fig. S5** for isothermal carbonation at 150 °C).

Temperature-programmed carbonation of MgO promoted with LiNO₃, NaNO₃, (Na,K)NO₃ and (Li,Na,K)NO₃ was also probed by *in situ* DRIFTS (**Fig. 3**, same conditions as the TGA experiments reported in **Fig 2a**). The analysis of the low frequency region of the infrared spectra of the materials allowed to track the evolution and emergence of peaks due to nitrates and carbonates. In all of the samples, the peak at 836 cm⁻¹, attributable to the out-of-plane bending of NO₃⁻ shifted to lower wavenumbers, 825 cm⁻¹, and broaden, upon heating, owing to melting of the salt (and in the case of NaNO₃ the $R\bar{3}c \rightarrow R\bar{3}m$ phase transition from an ordered to a disordered rhombohedral structure)⁵². The emergence of peaks due to the ν_1 , ν_2 and ν_4 modes of the CO₃²⁻ ion is associated with carbonation. For MgO-LiNO₃ (**Fig. 3a**) and MgO-(Na,K)NO₃ (**Fig. 3c**), the evolution of these peaks confirms a gradual increase of CO₂ sorption from 250 °C onwards, while MgO-NaNO₃ (**Fig. 3b**) shows fast carbonation in the temperature range 300 - 350 °C. For MgO-(Li,Na,K)NO₃ (**Fig. 3d**), the DRIFTS analysis confirms that carbonation proceeds already at 150 °C (emergence of a shoulder at 879 cm⁻¹; out-of-plane bending motion (ν_2) of the carbonate ion), in line with the observations made by TGA shown in **Fig. S5**.

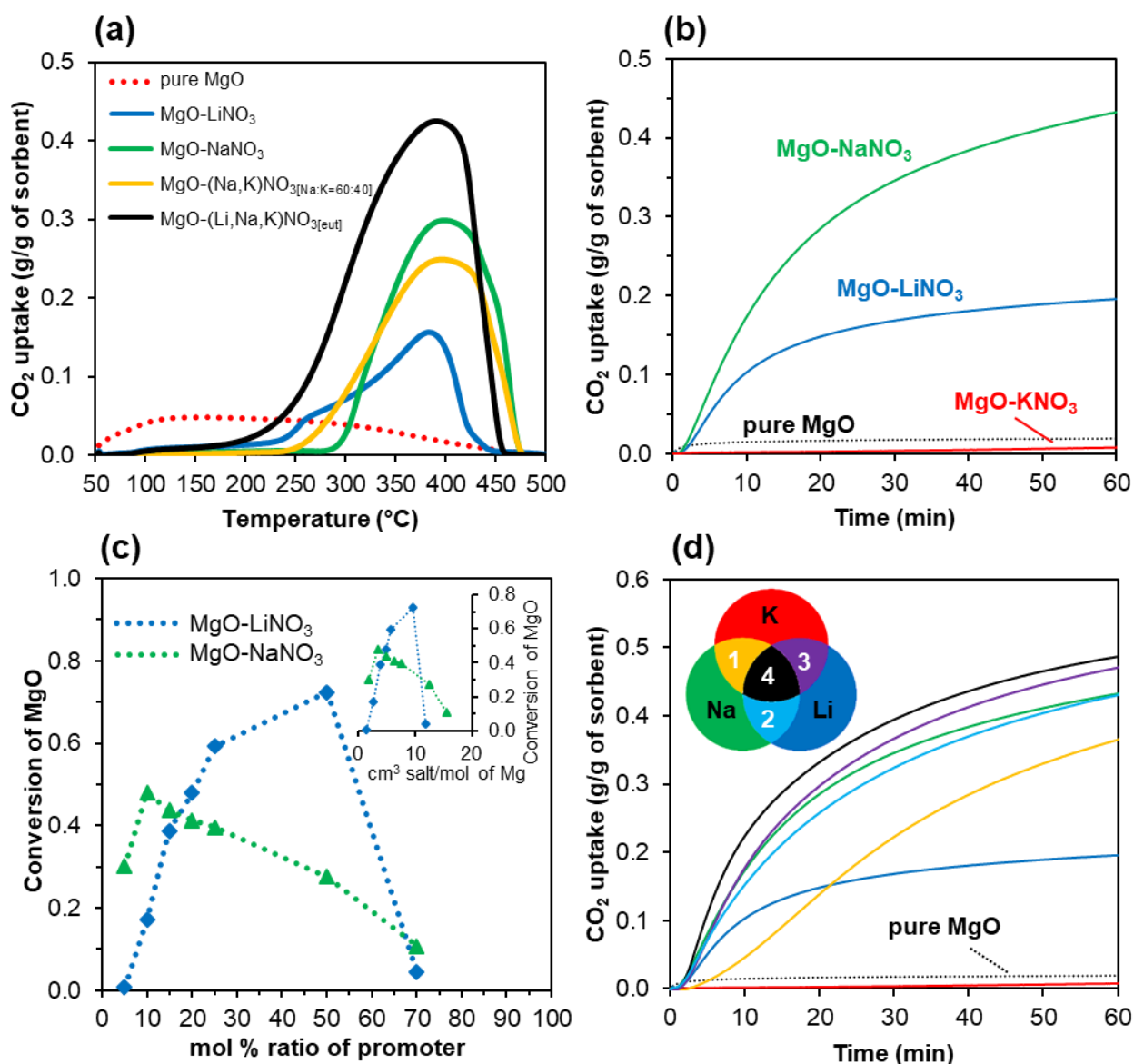


Fig. 2: CO₂ uptake of a series of MgO-based sorbents: **a)** CO₂ uptake of MgO promoted by 10 mol % alkali metal nitrate during heating in CO₂ at a ramp rate of 10 °C/min; **b)** CO₂ uptake of MgO promoted with different alkali metal nitrates (LiNO₃, NaNO₃, KNO₃) at 300 °C in CO₂; **c)** conversion of MgO promoted with different amounts of LiNO₃ or NaNO₃ after 1 h carbonation in CO₂ at 300 °C. Inset plots the conversion of MgO as a function of volume of promoter added per mol of Mg; and **d)** CO₂ uptake of MgO promoted with eutectic mixtures of alkali metal nitrates: 1. (Na,K)NO₃, 2. (Li,Na)NO₃, 3. (Li,K)NO₃, and 4. (Li,Na,K)NO₃, carbonation in CO₂ at 300 °C compared to pure MgO and MgO promoted by the individual nitrates.

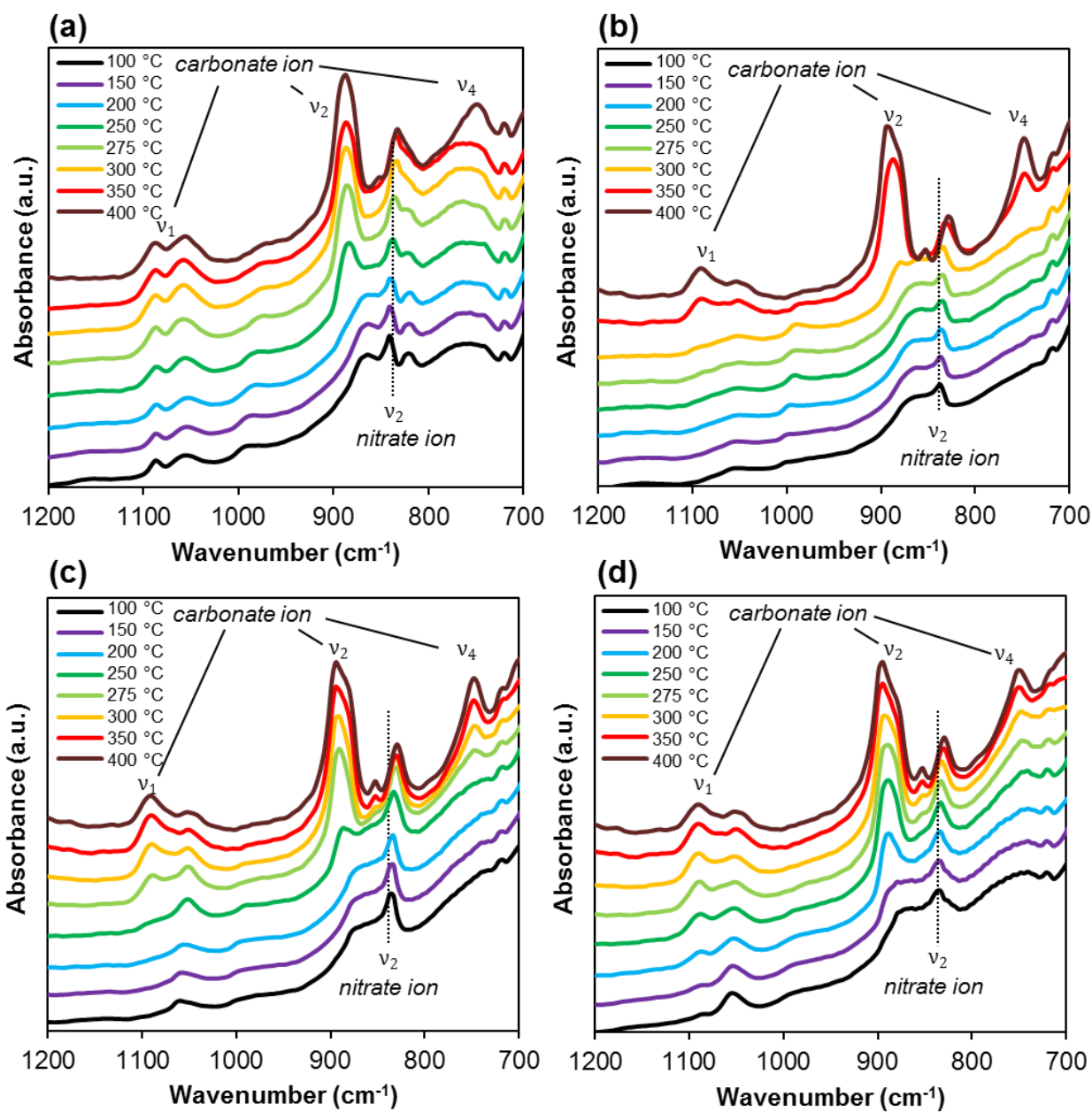


Fig. 3: *In situ* DRIFTS spectra of MgO promoted with **a)** 10 mol % LiNO₃, **b)** 10 mol % NaNO₃, **c)** 10 mol % (Na,K)NO₃ (Na:K ratio = 60:40), **d)** 10 mol % (Li,Na,K)NO₃ (eutectic composition) during heating in CO₂ using a ramp rate of 10 °C/min.

3.2.3 Isothermal CO₂ sorption by promoted MgO

To obtain a qualitative understanding of the effect of different promoters on the carbonation kinetics, **Fig. 2b** plots the isothermal CO₂ uptake at 300 °C of a series of MgO samples that were promoted with 10 mol % of different alkali metal nitrates as a function of time. Carbonation of unpromoted MgO occurs in the first few minutes, albeit reaching very rapidly an asymptotic limit of 19 mg CO₂/g sorbent owing to limitations due to product layer diffusion. On the other hand, the carbonation of promoted MgO samples (with LiNO₃ or NaNO₃) is initially slower. Yet, after an induction period of ~2 min the rate of carbonation accelerated appreciably, leading to a high CO₂ uptake. MgO-LiNO₃ and MgO-NaNO₃ yield CO₂ uptakes of 196 and 432 mg CO₂/g sorbent, respectively. As expected, MgO promoted by KNO₃ did not show any notable carbonation owing to the high melting point of KNO₃ (MP = 334 °C). The binding of CO₂ on a MgO surface during the isothermal carbonation of both NaNO₃-promoted and unpromoted MgO was examined further by *in situ* DRIFTS. **Figs. S6-S8** in the SI demonstrate that on bare MgO only a surface layer of monodentate carbonates form, whereas vibrations due to carbonate ions are present for promoted MgO.

We also observe that the quantity of promoter added to the sorbent has a substantial impact on the extent of carbonation of MgO. **Fig. 2c** explores the effect of molar content of the alkali nitrate on the CO₂ uptake of LiNO₃- and NaNO₃-promoted MgO. For LiNO₃-promoted MgO, the extent of carbonation of MgO increased when the ratio of LiNO₃ to MgO increased from 5 to 50 mol %, followed by a remarkable decline when the content of LiNO₃ reached 70 mol %. For NaNO₃-promoted MgO, the optimal molar ratio of NaNO₃ was determined as 10 mol %, with the extent of carbonation of MgO decreasing almost linearly with increasing quantities of NaNO₃ for higher loadings. For both promoters, it appears that an increase in the quantity of the promoter enhances the carbonation of MgO, presumably by increasing the interfacial area between MgO and the promoter, thus increasing the surface of MgO available for reaction. Once a certain thickness of the molten layer is reached, the mass transfer resistance for CO₂ may increase appreciably.

Fig. 2d extends the analysis of **Fig. 2b**, by exploring the effect of binary and ternary eutectics with different melting points on the carbonation of MgO at 300 °C. MgO promoted with an eutectic mixture of (Na,K)NO₃ (MP = 221 °C) exhibited the slowest kinetics, yielding a CO₂ uptake of 365 mg CO₂/g sorbent, lower than that of MgO-NaNO₃, which is in agreement with previously reported results²³. The eutectic mixtures (Li,Na)NO₃ (MP = 200 °C) and (Li,K)NO₃ (MP = 130 °C) promoted appreciably the CO₂ uptake of MgO yielding CO₂ uptakes of 433 and 470 mg CO₂/g sorbent, respectively. Promotion with the eutectic, ternary mixture (Li,Na,K)NO₃ (MP = 120 °C) gave the highest CO₂ uptake of 474 mg CO₂/g sorbent.

To explore the general validity of nitrate promotion, isothermal carbonation experiments were performed for nitrate-promoted CaO. These experiments demonstrate an improved CO₂ capture performance of promoted CaO compared to unpromoted CaO (see **Figs. S9-S11** and related discussion in the SI).

3.3 CO₂ uptake kinetics and reaction mechanism

Examining the CO₂ sorption kinetics (**Fig. 4a**), of a representative sample of promoted MgO (MgO - 10 mol % NaNO₃), it appears that the carbonation proceeds through four distinct stages: i) an initial, rapid, but brief carbonation stage, resembling the behavior of uncoated MgO, ii) an abrupt levelling-

off of the CO₂ uptake, iii) a reaction stage with an accelerated rate of carbonation and iv) a final stage characterized by a slow, but continuous decline of the carbonation activity, preventing the full conversion of the sorbent. The intermediate stage iii that lasts approximately 4-5 min distinguishes the behavior of promoted MgO samples from pure MgO. The MgO conversion profile in stage iii, as shown in **Fig. 4b**, can be interpreted by the Avrami model for reactions governed by nucleation-and-growth dynamics ⁵³:

$$\frac{dX}{dt} = k \cdot n(1 - X)(-\ln(1 - X))^{1-\frac{1}{n}} \quad (2)$$

where X is the fractional conversion of the sorbent, k is the apparent reaction rate (s⁻¹) and n a power index (assumed as 2). The agreement between the experimental data and the model suggests that the nucleation and growth of MgCO₃ crystals is the controlling process in stage iii.

In the reaction stage ii (induction time), the accumulation of the rate-limiting species for carbonation takes place. As mentioned in the Introduction, the rate-limiting step is considered to be either 1) the formation of CO₃²⁻ ions (owing to the solubility of CO₂ and the high concentration of O²⁻ ions in the molten nitrate), or 2) the formation of Mg²⁺ ions through the dissolution of MgO in the molten promoter. Once a critical concentration of the ions has been reached, the rapid nucleation of MgCO₃ crystals, i.e. stage iii, takes over.

To assess the validity of these two hypotheses, the dissolution of MgO in LiNO₃, NaNO₃ and the ternary eutectic mixture (Li,Na,K)NO₃ was assessed via the immersion of a MgO single crystal in a crucible of molten salts at 350 °C for 10 h. The amount of Mg retained in the salt after cooling down, expressed as a molar ratio of Mg to the cations of the nitrate, was quantified by ICP-OES. For the LiNO₃ and the NaNO₃ melt, the molar ratio of Mg to Li and Na was 1.42 x 10⁻⁴ and 1.75 x 10⁻⁴, respectively. For the ternary mixture, the ratio n(Mg)/(n(Li)+n(Na)+n(K)) was equal to 2.25 x 10⁻⁴. As shown in the inset of **Fig. 4b**, the apparent reaction rate constants k obtained from **Fig. 4b** for MgO-LiNO₃, MgO-NaNO₃ and MgO-(Li,Na,K)NO₃ correlate well with the amount of Mg²⁺ dissolved in the respective nitrates. Overall, our findings support the hypothesis that the rate of MgCO₃ nucleation and consequently, the rate of CO₂ uptake is controlled by the dissolution and accumulation of Mg²⁺ in the molten promoter. Previously, this hypothesis has been supported only through density functional theory calculations ^{21,34}. Conversely, our results do not support the hypothesis that the carbonation reaction is controlled by the solubility of CO₂ in the molten promoter. According to previous reports ^{54,55}, the solubility of CO₂ in molten alkali metal nitrates should increase with decreasing ionic radius of the alkali metal cation (see also **Fig. S12**). Hence, one would expect that MgO-LiNO₃ exhibits the highest CO₂ uptake rate, yet it shows the lowest. In addition, the observation that also molten alkali metal chlorides show an appreciable promotion effect (with reference to CaO as a sorbent, see **Fig. S10**) suggests that a high concentration of O²⁻ ions (hypothesized to be present in molten nitrates) is not a necessary condition for the promotion of carbonation. Of course, it cannot be excluded that the solubility of CO₂ and rapid formation of CO₃²⁻ ions in molten nitrates play a role in the reaction kinetics (in particular at later stages), but the mechanism controlling the initial reaction rate (stage iii) appears to be the formation of Mg²⁺ ions (by MgO dissolution in the molten promoter).

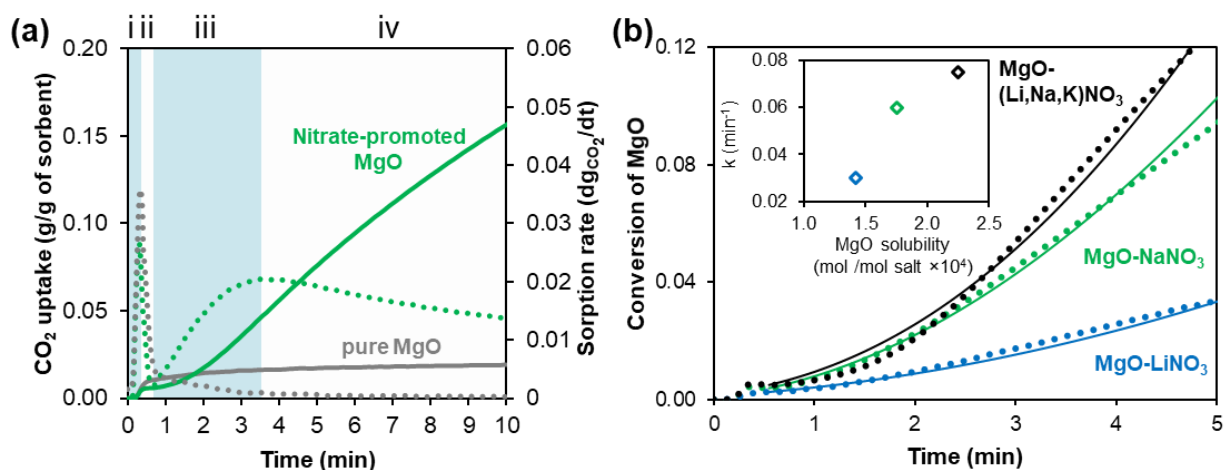


Fig. 4: **a)** Comparison of the CO₂ sorption kinetics of 10 mol % NaNO₃-promoted and pure MgO (continuous lines: cumulative CO₂ uptake, dashed lines: rate of CO₂ uptake). The CO₂ uptake profile of promoted MgO is divided into four reaction stages labelled i, ii, iii and iv. **b)** Experimental uptake of nitrate-promoted MgO samples in the reaction stage iii (dashed line) and predictions of the Avrami model (continuous lines). Inset: Correlation between the solubility of MgO in the nitrates (LiNO₃, NaNO₃ and ternary mixture as determined by ICP-OES measurements) and the apparent reaction rate k of the Avrami model.

3.4 Effect of melting point and composition of the nitrate mixture on the isothermal CO₂ uptake

Although all the nitrates tested that are in the molten state at the CO₂ capture conditions promote the reactivity of MgO, the extent of promotion was found to differ appreciably from salt to salt. Hence, to assess the dependence of the CO₂ uptake on the composition and the melting point of the nitrates (and mixtures thereof), a systematic study was performed. Here, the mole fraction of the promoter(s) was fixed to 10 mol % and binary mixtures of nitrates of different composition were tested for CO₂ capture at 300, 275 and 250 °C). **Fig. 5** plots the CO₂ uptake of MgO promoted by mixtures of (Na,K)NO₃, (Li,Na)NO₃ or (Li,K)NO₃ as a function of their melting point and composition. Analogously, **Fig. S13** shows the CO₂ uptake of MgO promoted by (Li,Na,K)NO₃ using a fixed quantity of Li and varying the ratio of Na : K.

For MgO-(Li,K)NO₃ we observed a correlation between the CO₂ uptake of the sorbent and the melting point of the promoter. At a given carbonation temperature, e.g., 300 °C, promoters with a lower melting point show a stronger enhancement of the CO₂ uptake. This could be linked to a higher mobility of ions in promoters with lower melting points.

In molten alkali metal nitrates, the viscosity (which generally relates inversely to the self-diffusivity of ions⁵⁶⁻⁵⁸) decreases with increasing temperature (**Fig. S14**). To (indirectly) confirm the role of ion mobility on the enhancement of the carbonation activity, **Fig. S15** shows the CO₂ uptake of MgO promoted with a ternary mixture of (Na,K)NO₃ and Ca(NO₃)₂. Ca(NO₃)₂ increases the viscosity of alkali metal nitrates and hence lowers the self-diffusion of ions in molten salts⁵⁹. In line with the previous argumentation, the rate of CO₂ uptake is reduced when Ca(NO₃)₂ was added to the promoting mixture.

However, the data presented in **Fig. 5** seem to indicate that the melting point of the promoter is not the only determinant for the CO₂ uptake of the sorbent. For MgO-(Na,K)NO₃ and MgO-(Li,Na)NO₃ the relationship between the CO₂ uptake and the melting point of the promoter is present but

somewhat “misaligned”, with higher CO₂ uptakes typically observed for higher Na contents. The best performing samples containing (Na,K)NO₃- and (Li,Na)NO₃ promoters have a higher Na content than the eutectic composition. At lower carbonation temperatures (275 °C and 250 °C), the effect of the higher Na content disappears and a clearer alignment between the CO₂ uptake and the melting point emerges. In light of the superior solubility of MgO in NaNO₃ compared to other nitrate salts (**Fig. 4**), it appears from **Fig. 5** that coating mixtures with a high Na content might benefit from the lower melting point compared to single nitrates (favoring ion dynamics of the reactant species) and the higher concentration of Mg²⁺ ions in molten NaNO₃.

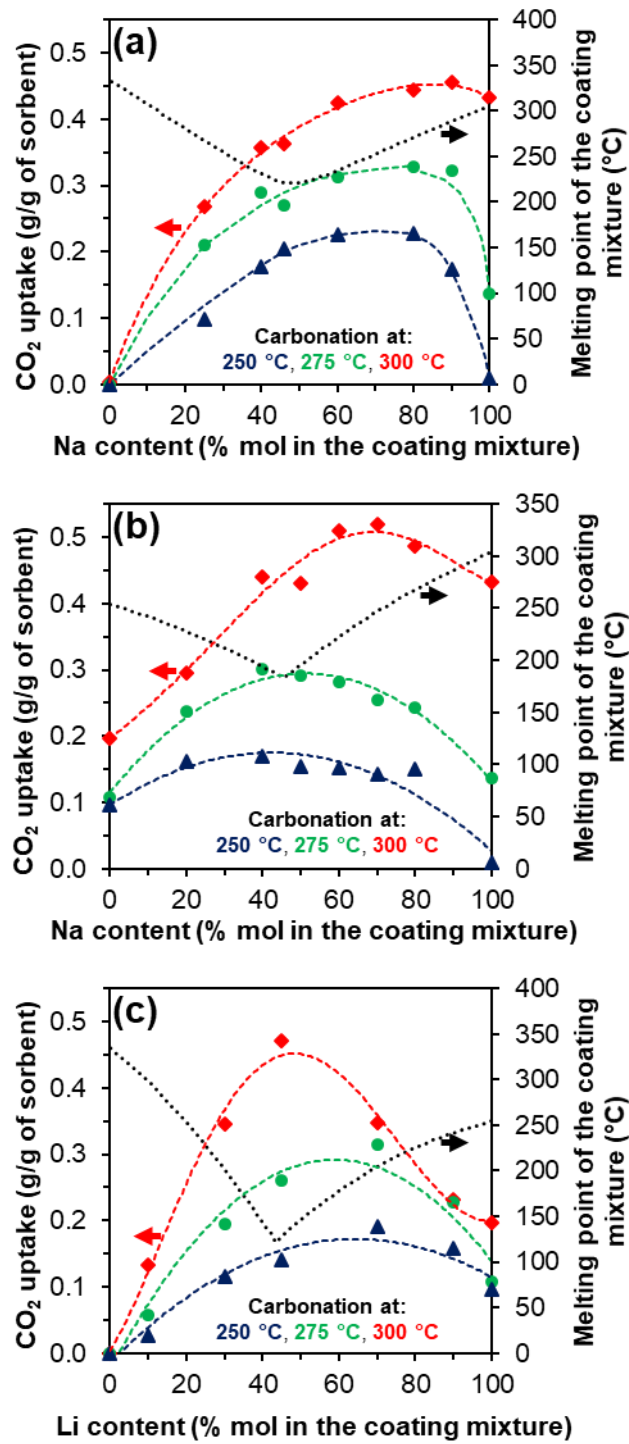


Fig. 5: CO₂ uptake after 1 h of carbonation: MgO promoted with 10 mol % of binary mixtures of alkali metal nitrates as a function of the composition of the coating mixture (and hence their melting point) at three different carbonation temperatures: **a)** (Na,K)NO₃, **b)** (Li,Na)NO₃, **c)** (Li,K)NO₃. Melting points of the mixtures according to reference ⁴¹.

3.5 Cyclic CO₂ uptake: deactivation and re-activation

3.5.1 Effect of sintering and nitrate segregation

The cyclic stability of the CO₂ uptake of nitrate-promoted MgO samples was assessed in a TGA by performing 10 cycles of repeated carbonation and regeneration, as shown in **Fig. 6a**. NaNO₃-promoted MgO showed a pronounced decay in the CO₂ uptake during the first 3 cycles, in agreement with previous findings^{21,22,50}. In contrast, the CO₂ uptake of MgO promoted by (Li,Na,K)NO₃ or LiNO₃ exhibited a rather gradual decline, yielding CO₂ uptakes of, respectively, 353 and 73 mg CO₂/g sorbent after 10 cycles. The cyclic CO₂ uptake of MgO promoted by binary mixtures of (Li,Na)NO₃ and (Li,K)NO₃ (**Fig. 6b**) was similar to that of the ternary mixture (Li,Na,K)NO₃ (the CO₂ uptake after 10 cycles was 340 and 344 mg CO₂/g sorbent for, respectively, (Li,Na)NO₃ and (Li,K)NO₃), while (Na,K)NO₃ rapidly lost its CO₂ uptake capacity, yielding only 44 mg CO₂/g sorbent after 10 cycles.

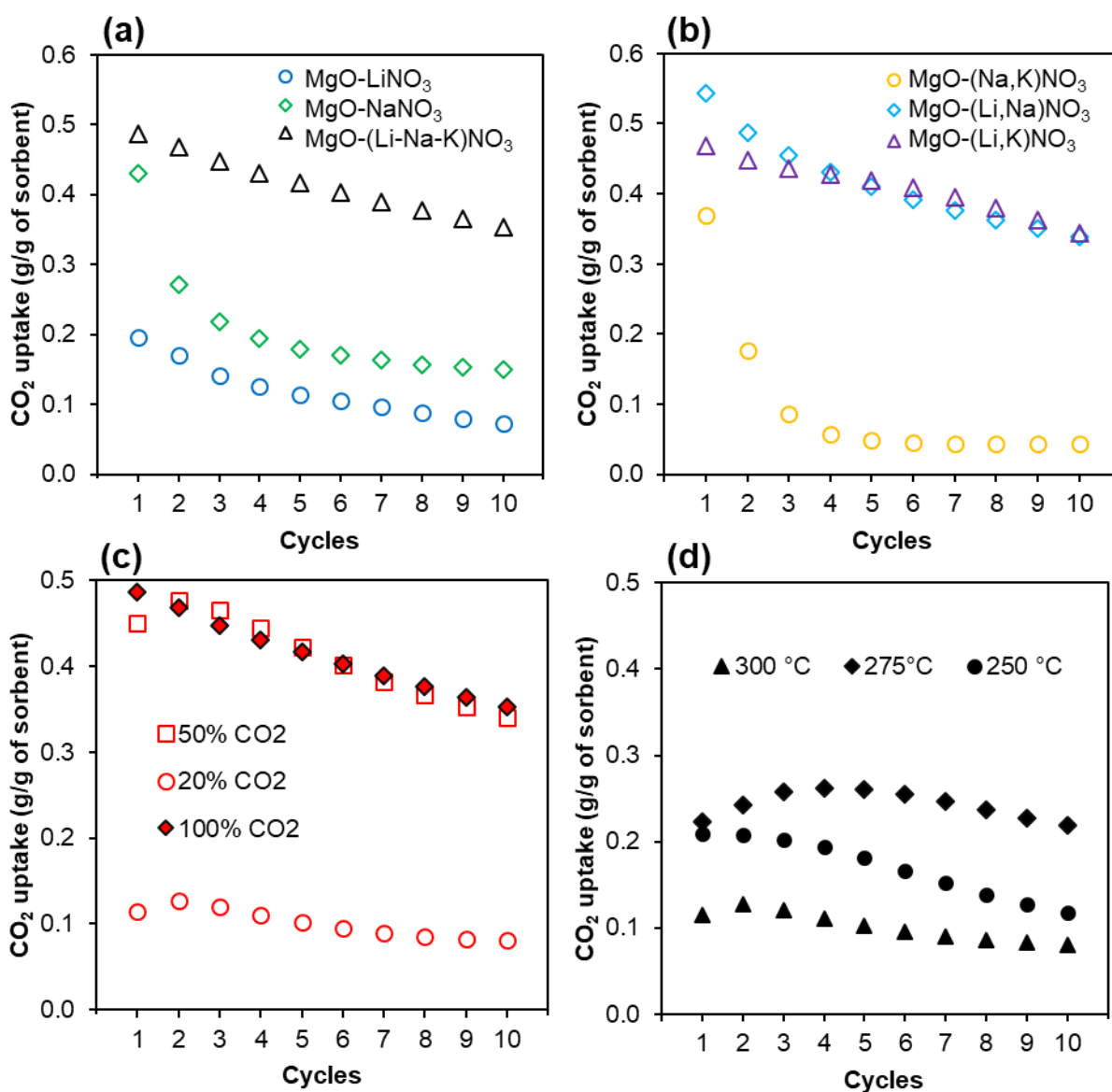


Fig. 6: CO₂ uptake of MgO promoted by 10 mol % alkali metal nitrates over 10 repeated cycles of carbonation and regeneration (carbonation at 300 °C in CO₂ and calcination at 450 °C in N₂): **a**) MgO promoted by NaNO₃, LiNO₃ or the ternary eutectic mixture (Li,Na,K)NO₃, **b**) samples

promoted with the most effective binary mixture of nitrates, as determined by a single carbonation step, see **Fig. 5, c**) cyclic performance of MgO promoted by 10 mol % (Li,Na,K)NO₃ under varying partial pressures of CO₂ at 300 °C, and **d**) cyclic performance of MgO promoted by 10 mol % (Li,Na,K)NO₃ for different carbonation temperatures at a partial pressure of CO₂ of 0.2 atm.

Next, we aimed to elucidate the underlying mechanism(s) for sorbent deactivation. The surface area and the pore volume of the fresh sorbents and after 10 cycles (regenerated state) are listed in **Table 2**. In addition, **Fig. 7a** shows the morphology of the samples prior to and after cyclic testing as probed by EDX-SEM. Table 2 confirms that promoted MgO loses its surface area and pore volume during cycling. The loss of surface area and pore volume occurs primarily in the first cycle (see **Fig. S16**). Interestingly, sintering appears to be more pronounced in samples that have shown, on average, a higher CO₂ uptake capacity. Specifically, MgO promoted by (LiNa,K)NO₃ or NaNO₃ exhibited a 65 % and 45 % reduction of their surface area, whereas LiNO₃-promoted MgO lost only 35 % of its surface area. This can be explained by the fact that the phase that is most likely subject to sintering, i.e. MgCO₃ (with its low Tammann temperature of ~ 180 °C³¹), is present in higher quantities in the samples that show a higher CO₂ uptake.

Table 2: Surface area and pore volume of MgO-based CO₂ sorbents as determined by N₂ physisorption experiments prior to and after cyclic testing (**Fig. 6a**).

Sample	BET surface area (m ² /g)		BJH pore volume (cm ³ /g)	
	before cycling	after 10 cycles	before cycling	after 10 cycles
MgO – LiNO ₃	28	17	0.22	0.13
MgO – NaNO ₃	27	15	0.19	0.04
MgO – (Li,Na,K)NO ₃	22	8	0.08	0.02

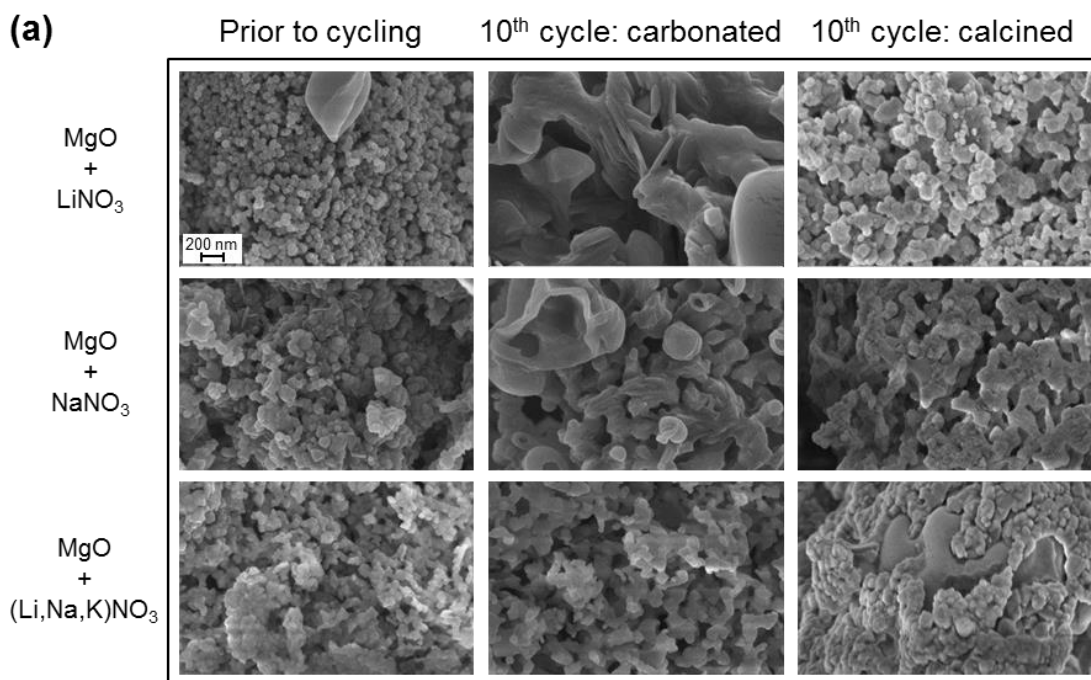
As there is not a direct relationship between the degree of sintering and the reduction of the CO₂ uptake, sintering alone cannot explain sorbent deactivation. Hence, it is likely that also some promoter-related deactivation occurs. As salts such as NaNO₃ do not decompose at the reaction temperatures used here⁴⁰, deactivation might be a consequence of surface segregation of the molten nitrate, leaving parts of the MgO surface uncovered. SEM-EDX images of the fresh sorbent before cycling shows a well-distributed nitrate phase (**Fig. S17**). On the other hand, after the first carbonation step, EDX mapping of MgO-NaNO₃ (**Fig. 7b**) shows a more heterogeneous distribution of NaNO₃ on the MgO surface (see also **Fig. S18**). Our experimental observation seems to support the hypothesis that, owing to the poor wettability of MgCO₃ with nitrates, the active surface area (i.e. the interface MgO-NaNO₃) reduces with cycle number.

3.5.2 Re-activation of spent nitrate-promoted MgO

Aiming at developing strategies to re-activate promoted MgO-based CO₂ sorbents, a series of experiments were carried out. First, a sample of MgO promoted by 10 mol % NaNO₃ was taken after 10 carbonation/calcination cycles (“cycled sample”) and the water-soluble NaNO₃ was removed by vacuum filtration through a polycarbonate membrane. The remaining MgO was then “recoated” by mixing it with 10 mol % NaNO₃ in a mortar and tested for an additional 10 cycles of carbonation and calcination. This process should remove the segregated NaNO₃ and substitute it with new, well-distributed NaNO₃. In order to isolate the contribution of the “re-coating” process to the re-activation of the sorbent (i.e. exposure of MgO to an aqueous environment), two additional control experiments were carried out: (i) mechanical grinding: re-grinding of the cycled sample taken at the 10th calcination step in a mortar, without washing and without addition of new fresh NaNO₃, and (ii) treatment with water: immersing the cycled sample (taken at the 10th calcination step) in water, without filtering or the addition of fresh NaNO₃, and drying at 80 °C. Therefore, the two control samples retained the “original” NaNO₃ of the sample, whereas in the “re-coated” sample the original NaNO₃ is removed and replaced with fresh NaNO₃.

As shown in **Fig. 8**, the CO₂ uptake in the 1st carbonation cycle after re-activation of the sorbent (“recoated” sample) is significantly higher than that in the last cycle before reactivation, yet lower than the CO₂ uptake of the fresh, initial material. The partial restoration of the CO₂ uptake capacity after the distribution of fresh NaNO₃ is an additional evidence that the loss in performance during cycling is not only due to the reduction of surface area and pore volume, but also due to morphological changes of the promoter.

On the other hand, the fact that some decay of the CO₂ uptake performance is due to material sintering (visible to some extent in the SEM images shown in **Fig. 7a**) is supported by the observation that the CO₂ uptake is not completely recovered after reactivation of the sorbent by the addition of fresh NaNO₃. The control experiments (i.e., grinding and rehydration) clarified whether sorbent reactivation can be achieved even without washing and “recoating” with fresh NaNO₃. As shown in **Fig. 8**, only a small recovery of the CO₂ uptake was observed after mechanical grinding. Conversely, reactivation by simple re-dispersion of the nitrate promoter using water, lead to a similar recovery of the CO₂ uptake as the “recoating” process. By first immersing the cycled sample in water and then slowly evaporating the water, the process induces the dissolution and re-deposition of the nitrate in the cycled sample. Besides the redistribution of the promoter, the addition of water also affects the texture of the sorbent. As shown in **Fig. S19**, after 10 cycles of carbonation/calcination the crystallite size of MgO in MgO-NaNO₃ has increased from 24 to 35 nm. After the addition of water and heating, the average crystallite size of MgO was reduced to 29 nm. The exact reason behind this reduction in crystallite size is currently unclear, but might be linked to the formation of Mg(OH)₂, which after calcination yields MgO of relative smaller crystallite size compared to the cycled material. Indeed, a similar effect has been observed for the hydration of CaO⁶⁰. To conclude, it seems that hydration of the de-activated sorbent is a promising route for sorbent reactivation.



(b)

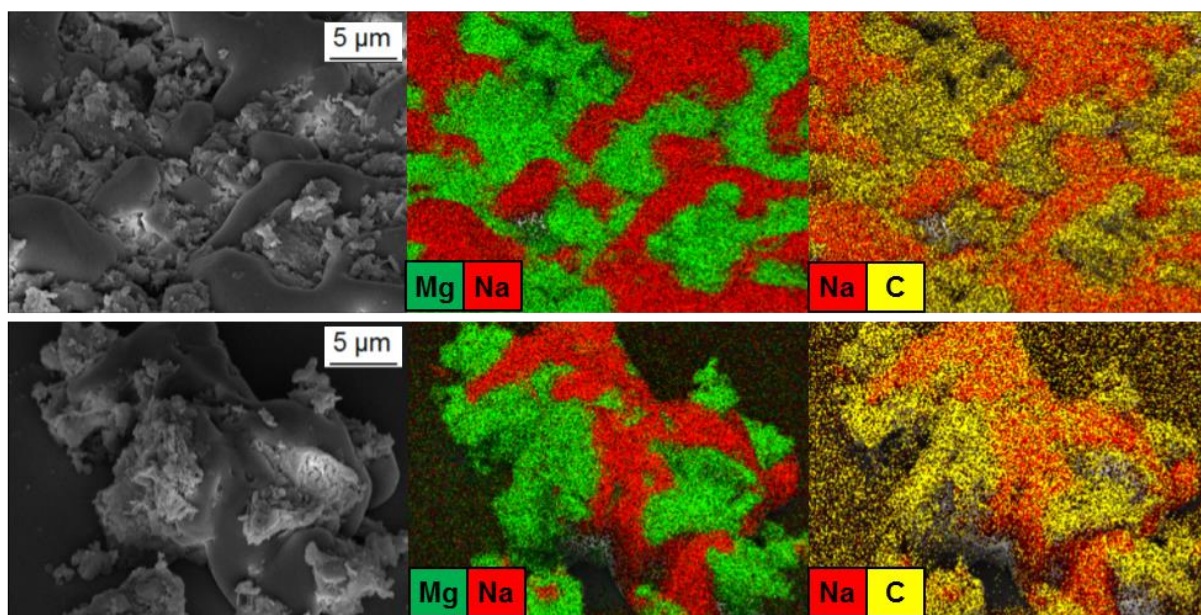


Fig. 7: **a)** SEM images of different CO₂ sorbents before cycling (calcined state), at the 10th cycle (carbonated state) and at the 10th cycle (calcined state) and **b)** SEM images and EDX mapping of of MgO promoted by 10 mol % NaNO₃ after 1 h of carbonation at 300 °C in CO₂.

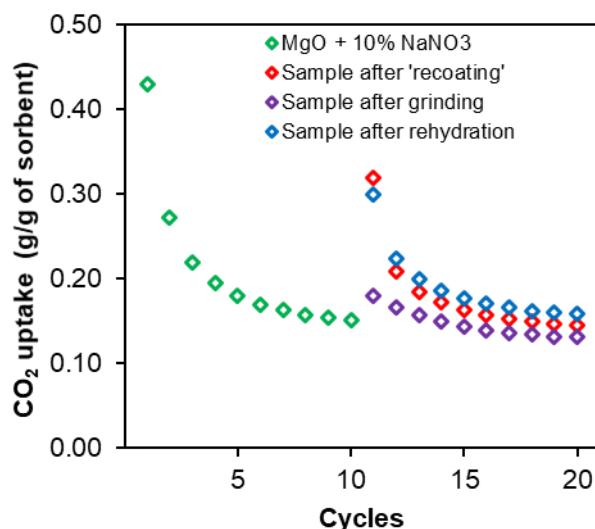


Fig. 8: Cyclic CO₂ uptake of NaNO₃-promoted MgO applying different re-activation approaches after the first 10 cycles (carbonation at 300 °C in CO₂ and calcination at 450 °C in N₂).

3.6 Discussion and implications for applications

Although it has been shown that the melting point of the promoter is a key determinant for the CO₂ capture performance, the data of **Fig. 5** and **Fig. S13** indicate that, especially for NaNO₃-containing mixtures, the CO₂ uptake remains high even when deviating from the eutectic ratios. This information is useful for industrial exploitation, for which material costs have to be minimized. The data acquired here provide the experimental basis to determine an optimum between material costs and CO₂ uptake. An additional issue with regards to the different pre- and post-combustion CO₂ capture applications are the diverse gas compositions. **Fig. 6c** plots the CO₂ uptake of the best CO₂ sorbent tested here (i.e., MgO-(Li,Na,K)NO₃) as a function of CO₂ partial pressure. Although the performance of the material in 50 vol. % CO₂ was comparable to the uptake obtained in pure CO₂, lowering the CO₂ concentration further (i.e., 20 vol. %) resulted in a sharp decrease in the CO₂ uptake, yielding an average value of 101 mg CO₂/g sorbent over 10 cycles. The CO₂ uptake in an atmosphere of 20 vol. % CO₂ was assessed also as a function of the carbonation temperature (**Fig. 6d**). Lowering the reaction temperature to 275 °C resulted in a doubling of the CO₂ uptake (average value of 243 mg CO₂/g sorbent over 10 cycles). This observation might be explained by the higher thermodynamic driving force at lower carbonation temperatures. In this context, eutectic mixtures become particularly interesting as the low melting point broadens the operating window of the material. Furthermore, under realistic conditions, the presence of steam in the CO₂ stream has to be considered. In **Fig. S20** we compare the performance of the best material tested here, i.e. MgO-(Li,Na,K)NO₃ with and without the presence of steam. Although the presence of steam improves slightly the CO₂ uptake in the first cycles, the CO₂ carrying capacity is reduced from cycle number six onwards. The mechanism behind this steam-induced deactivation is currently unclear and will require further investigation.

4 CONCLUSIONS

The CO₂ uptake and the cyclic stability of MgO promoted by alkali metal nitrates was studied in detail. It was demonstrated that the addition of nitrate salts to the MgO precursor affects both the microstructure (triggering the formation of larger MgO crystallites) and the CO₂ capture performance of the sorbent (significantly enhanced compared to bare MgO).

NaNO₃ was identified as the salt with the highest promoting effect on the carbonation of MgO. We attribute this to the higher solubility of MgO in NaNO₃, leading in turn to a faster formation of Mg²⁺, which appears to be the rate-limiting step of nitrate-mediated carbonation.

Eutectic mixtures of nitrates were shown to improve further the CO₂ uptake performance of MgO, by both increasing the solubility of MgO in the promoter and providing fast ion dynamics in the melt. In addition, the low melting point of eutectic mixtures enables a wider operation window of the CO₂ capture process.

The CO₂ uptake of nitrate-promoted MgO decays with number of carbonation/calcination cycles. MgO is subject to sintering, but a direct relationship between the extent of sintering and the cyclic CO₂ uptake was not observed. Instead, SEM-EDX indicates that upon carbonation the promoter migrates and segregates on the surface, reducing the active surface area. The loss in the CO₂ carrying capacity can be restored partially via a simple hydration approach.

The results reported here have advanced our understanding of the factors that determine the CO₂ uptake and the cyclic stability of nitrate-promoted MgO, thus providing useful insight for the further improvement of the formulation and synthesis protocols of MgO-based CO₂ sorbents.

ACKNOWLEDGMENTS

Alessandro Dal Pozzo would like to thank the “Marco Polo” scholarship program of the University of Bologna for providing the financial support for his research stay at ETH Zürich. The FIRST Center for Micro- and Nanoscience at ETH Zürich is acknowledged for providing access to electron microscopy. The authors would also thank Prof. André R. Studart for providing access to SEM/EDX and Financial support from Swiss National Science Foundation (SNSF, 200020_156015) is greatly acknowledged.

REFERENCES

- (1) Canadell, J. G.; Le Quéré, C.; Raupach, M. R.; Field, C. B.; Buitenhuis, E. T.; Ciais, P.; Conway, T. J.; Gillett, N. P.; Houghton, R.; Marland, G. Contributions to accelerating atmospheric CO₂ growth from economic activity, carbon intensity, and efficiency of natural sinks. *Proc. Natl. Acad. Sci. U. S. A.* **2007**, 104, 18866-18870.
- (2) Betts, R. A.; Jones, C. D.; Knight, J. R.; Keeling, R. F.; Kennedy, J. J. El Niño and a record CO₂ rise. *Nat. Clim. Change* **2016**, 6, 806.
- (3) Choi, S.; Drese, J. H.; Jones, C. W. Adsorbent materials for carbon dioxide capture from large anthropogenic point sources. *ChemSusChem* **2009**, 2, 796-854.
- (4) MacDowell, N.; Florin, N.; Buchard, A.; Hallett, J.; Galindo, A.; Jackson, G.; Adjiman, C. S.; Williams, C. K.; Shah, N.; Fennell, P. An overview of CO₂ capture technologies. *Energy Environ. Sci.* **2010**, 3, 1645-1669.
- (5) Wang, S.; Yan, S.; Ma, X.; Gong, J. Recent advances in capture of carbon dioxide using alkali-metal-based oxides. *Energy Environ. Sci.* **2011**, 4, 3805-3819.
- (6) Wang, J.; Huang, L.; Yang, R.; Zhang, Z.; Wu, J.; Gao, Y.; Wang, Q.; O'Hare, D.; Zhong, Z. Recent advances in solid sorbents for CO₂ capture and new development trends. *Energy Environ. Sci.* **2014**, 7, 3478-3518.
- (7) Dal Pozzo, A.; Armutlulu, A.; Rekhina, M.; Müller, C. R.; Cozzani, V. CO₂ Uptake Potential of Ca-Based Air Pollution Control Residues over Repeated Carbonation–Calcination Cycles. *Energy Fuels* **2018**, 32, 5386–5395.
- (8) Blamey, J.; Anthony, E.; Wang, J.; Fennell, P. The calcium looping cycle for large-scale CO₂ capture. *Prog. Energy Combust. Sci.* **2010**, 36, 260-279.
- (9) Kierzkowska, A. M.; Pacciani, R.; Müller, C. R. CaO-Based CO₂ Sorbents: From Fundamentals to the Development of New, Highly Effective Materials. *ChemSusChem* **2013**, 6, 1130-1148.
- (10) Armutlulu, A.; Naeem, M. A.; Liu, H.-J.; Kim, S. M.; Kierzkowska, A.; Fedorov, A.; Müller, C. R. Multishelled CaO Microspheres Stabilized by Atomic Layer Deposition of Al₂O₃ for Enhanced CO₂ Capture Performance. *Adv. Mat.* **2017**, 29, 1702896.
- (11) Naeem, M. A.; Armutlulu, A.; Imtiaz, Q.; Müller, C. R. CaO-Based CO₂ Sorbents Effectively Stabilized by Metal Oxides. *ChemPhysChem* **2017**, 18, 3280-3285.
- (12) Martínez, A.; Lara, Y.; Lisbona, P.; Romeo, L. M. Energy penalty reduction in the calcium looping cycle. *Int. J. Greenhouse Gas Control* **2012**, 7, 74-81.
- (13) Dunstan, M. T.; Jain, A.; Liu, W.; Ong, S. P.; Liu, T.; Lee, J.; Persson, K. A.; Scott, S. A.; Dennis, J. S.; Grey, C. P. Large scale computational screening and experimental discovery of novel materials for high temperature CO₂ capture. *Energy Environ. Sci.* **2016**, 9, 1346-1360.
- (14) Ida, J.-I.; Lin, Y. Mechanism of high-temperature CO₂ sorption on lithium zirconate. *Environ. Sci. Technol.* **2003**, 37, 1999-2004.
- (15) Qi, Z.; Daying, H.; Yang, L.; Qian, Y.; Zibin, Z. Analysis of CO₂ sorption/desorption kinetic behaviors and reaction mechanisms on Li₄SiO₄. *AIChE J.* **2013**, 59, 901-911.
- (16) Zarghami, S.; Hassanzadeh, A.; Arastoopour, H.; Abbasian, J. Effect of Steam on the Reactivity of MgO-Based Sorbents in Precombustion CO₂ Capture Processes. *Ind. Eng. Chem. Res.* **2015**, 54, 8860-8866.
- (17) Gregg, S.; Ramsay, J. Adsorption of carbon dioxide by magnesia studied by use of infrared and isotherm measurements. *J. Chem. Soc. A* **1970**, 2784-2787.
- (18) Fagerlund, J.; Highfield, J.; Zevenhoven, R. Kinetics studies on wet and dry gas–solid carbonation of MgO and Mg(OH)₂ for CO₂ sequestration. *RSC Adv.* **2012**, 2, 10380-10393.
- (19) Ding, Y.-D.; Song, G.; Liao, Q.; Zhu, X.; Chen, R. Bench scale study of CO₂ adsorption performance of MgO in the presence of water vapor. *Energy* **2016**, 112, 101-110.

- (20) Vu, A.-T.; Park, Y.; Jeon, P. R.; Lee, C.-H. Mesoporous MgO sorbent promoted with KNO₃ for CO₂ capture at intermediate temperatures. *Chem. Eng. J.* **2014**, *258*, 254-264.
- (21) Zhang, K.; Li, X. S.; Li, W. Z.; Rohatgi, A.; Duan, Y.; Singh, P.; Li, L.; King, D. L. Phase Transfer-Catalyzed Fast CO₂ Absorption by MgO-Based Absorbents with High Cycling Capacity. *Adv. Mat. Interfaces* **2014**, *1*.
- (22) Prashar, A. K.; Seo, H.; Choi, W. C.; Kang, N. Y.; Park, S.; Kim, K.; Min, D. Y.; Kim, H. M.; Park, Y. K. Factors affecting the rate of CO₂ absorption after partial desorption in NaNO₃-promoted MgO. *Energy Fuels* **2016**, *30*, 3298-3305.
- (23) Harada, T.; Simeon, F.; Hamad, E. Z.; Hatton, T. A. Alkali metal nitrate-promoted high-capacity MgO adsorbents for regenerable CO₂ capture at moderate temperatures. *Chem. Mat.* **2015**, *27*, 1943-1949.
- (24) Yang, X.; Zhao, L.; Xiao, Y. Effect of NaNO₃ on MgO–CaCO₃ absorbent for CO₂ capture at warm temperature. *Energy Fuels* **2013**, *27*, 7645-7653.
- (25) Zhang, K.; Li, X. S.; Chen, H.; Singh, P.; King, D. L. Molten salt promoting effect in double salt CO₂ absorbents. *J. Phys. Chem. C* **2015**, *120*, 1089-1096.
- (26) Kim, S.; Jeon, S. G.; Lee, K. B. High-temperature CO₂ sorption on hydrotalcite having a high Mg/Al molar ratio. *ACS Appl. Mat. Interfaces* **2016**, *8*, 5763-5767.
- (27) Harada, T.; Hatton, T. A. Colloidal nanoclusters of MgO coated with alkali metal nitrates/nitrites for rapid, high capacity CO₂ capture at moderate temperature. *Chem. Mat.* **2015**, *27*, 8153-8161.
- (28) Vu, A.-T.; Ho, K.; Jin, S.; Lee, C.-H. Double sodium salt-promoted mesoporous MgO sorbent with high CO₂ sorption capacity at intermediate temperatures under dry and wet conditions. *Chem. Eng. J.* **2016**, *291*, 161-173.
- (29) Wang, L.; Zhou, Z.; Hu, Y.; Cheng, Z.; Fang, X. Nanosheet MgO-Based CO₂ Sorbent Promoted by Mixed-Alkali-Metal Nitrate and Carbonate: Performance and Mechanism. *Ind. Eng. Chem. Res.* **2017**, *56*, 5802-5812.
- (30) Cui, H.; Zhang, Q.; Hu, Y.; Peng, C.; Fang, X.; Cheng, Z.; Galvita, V. V.; Zhou, Z. Ultrafast and Stable CO₂ Capture Using Alkali Metal Salt-Promoted MgO–CaCO₃ Sorbents. *ACS Appl. Mat. Interfaces* **2018**, *10*, 20611-20620.
- (31) Zhao, X.; Ji, G.; Liu, W.; He, X.; Anthony, E. J.; Zhao, M. Mesoporous MgO promoted with NaNO₃/NaNO₂ for rapid and high-capacity CO₂ capture at moderate temperatures. *Chem. Eng. J.* **2018**, *332*, 216-226.
- (32) Hwang, B. W.; Lim, J. H.; Chae, H. J.; Ryu, H.-J.; Lee, D.; Lee, J. B.; Kim, H.; Lee, S. C.; Kim, J. C. CO₂ capture and regeneration properties of MgO-based sorbents promoted with alkali metal nitrates at high pressure for the sorption enhanced water gas shift process. *Proc. Saf. Environ. Prot.* **2018**, *116*, 219-227.
- (33) Qiao, Y.; Wang, J.; Zhang, Y.; Gao, W.; Harada, T.; Huang, L.; Hatton, T. A.; Wang, Q. Alkali Nitrates Molten Salt Modified Commercial MgO for Intermediate-Temperature CO₂ Capture: Optimization of the Li/Na/K Ratio. *Ind. Eng. Chem. Res.* **2017**, *56*, 1509–1517.
- (34) Lee, H.; Triviño, M. L. T.; Hwang, S.; Kwon, S. H.; Lee, S. G.; Moon, J. H.; Yoo, J.; Seo, J. G. In Situ Observation of Carbon Dioxide Capture on Pseudo-Liquid Eutectic Mixture-Promoted Magnesium Oxide. *ACS Appl. Mat. Interfaces* **2018**, *10*, 2414-2422.
- (35) Kou, X.; Guo, H.; Ayele, E.G.; Li, S.; Zhao, Y.; Wang, S.; Ma, X. Adsorption of CO₂ on MgAl–CO₃ LDHs-Derived Sorbents with 3D Nanoflower-like Structure. *Energy Fuels* **2018**, *32*, 5313-5320.

- (36) Jin, S.; Ko, K.-J.; Song, Y.-G.; Lee, K.; Lee, C.-H. Fabrication and kinetic study of spherical MgO agglomerates via water-in-oil method for pre-combustion CO₂ capture. *Chem. Eng. J.* **2019**, 359, 285–297.
- (37) Naeem, M. A.; Armutlulu, A.; Broda, M.; Lebedev, D.; Muller, C. R. The development of effective CaO-based CO₂ sorbents via a sacrificial templating technique. *Faraday Discuss.* **2016**, 192, 85-95.
- (38) Naeem, M. A.; Armutlulu, A.; Imtiaz, Q.; Donat, F.; Schäublin, R.; Kierzkowska, A.; Müller, C. R. Optimization of the structural characteristics of CaO and its effective stabilization yield high-capacity CO₂ sorbents. *Nat. Comm.* **2018**, 9, 2408.
- (39) Jo, S.-I.; An, Y.-I.; Kim, K.-Y.; Choi, S.-Y.; Kwak, J.-S.; Oh, K.-R.; Kwon, Y.-U. Mechanisms of absorption and desorption of CO₂ by molten NaNO₃-promoted MgO. *Phys. Chem. Chem. Phys.* **2017**, 19, 6224-6232.
- (40) Stern, K. H. High temperature properties and thermal decomposition of inorganic salts with oxyanions, CRC press, **2000**.
- (41) Coscia, K.; Elliott, T.; Mohapatra, S.; Oztekin, A.; Neti, S. Binary and ternary nitrate solar heat transfer fluids. *J. Sol. Energy Eng.* **2013**, 135, 021011.
- (42) Janz, G. J.; Allen, C. B.; Downey Jr, J. R.; Tomkins, R. Physical properties data compilations relevant to energy storage. I. Molten salts: Eutectic Data. Technical report, National Standard Reference Data System, **1978**.
- (43) Bradshaw, R.; Meeker, D. High-temperature stability of ternary nitrate molten salts for solar thermal energy systems. *Sol. Energy Mat.* **1990**, 21, 51-60.
- (44) Rodríguez-Carvajal, J. Recent Advances in Magnetic Structure Determination by Neutron Powder Diffraction. *Physica B* **1993**, 192, 55–69.
- (45) Hänchen, M.; Prigiobbe, V.; Baciocchi, R.; Mazzotti, M. Precipitation in the Mg-carbonate system—effects of temperature and CO₂ pressure. *Chem. Eng. Sci.* **2008**, 63, 1012-1028.
- (46) Hu, J.; Zhu, K.; Chen, L.; Kübel, C.; Richards, R. MgO (111) nanosheets with unusual surface activity. *J. Phys. Chem. C* **2007**, 111, 12038-12044.
- (47) Downing, C.; Sokol, A.; Catlow, C. The reactivity of CO₂ on the MgO (100) surface. *Phys. Chem. Chem. Phys.* **2014**, 16, 184-195.
- (48) Yang, Y.; Asta, M.; Laird, B. B. Solid-liquid interfacial premelting. *Phys. Rev. Lett.* **2013**, 110, 096102.
- (49) Zhang, K.; Li, X. S.; Duan, Y.; King, D. L.; Singh, P.; Li, L. Roles of double salt formation and NaNO₃ in Na₂CO₃-promoted MgO absorbent for intermediate temperature CO₂ removal. *Int. J. Greenhouse Gas Control* **2013**, 12, 351-358.
- (50) Janz, G.; Kelly, F.; Perano, J. Melting and Pre-Melting Phenomena in Alkali Metal Nitrates. *J. Chem. Eng. Data* **1964**, 9, 133-136.
- (51) Lee, H. J.; Kim, J. H.; Kim, J. W.; Cho, S. J. Structure Transformation of Na-Mg Based Salts for CO₂ Capture and Storage at High Temperature Probed with Variable Temperature X-ray Powder Diffraction. *Energy Procedia* **2014**, 63, 253-265.
- (52) Harris, M. J.; Salje, E. K.; Guttler, B. An infrared spectroscopic study of the internal modes of sodium nitrate: implications for the structural phase transition. *J. Phys.: Condens. Matter* **1990**, 2, 5517.
- (53) Khawam, A.; Flanagan, D. R. Solid-state kinetic models: basics and mathematical fundamentals. *J. Phys. Chem. B* **2006**, 110, 17315-17328.
- (54) Novozhilov, A.; Bamburov, V.; Fedotova, N. Solubility of carbon dioxide in molten alkali-metal nitrates. *Russ. J. Inorg. Chem.* **2007**, 52, 1679-1681.

- (55) Sada, E.; Katoh, S.; Yoshii, H.; Takemoto, I.; Shiomi, N. Solubility of Carbon Dioxide in Molten Alkali Halides and Nitrates and Their Binary Mixtures. *J. Chem. Eng. Data* **1981**, *26*, 279.
- (56) Van Loef, J. J. Hard-sphere Results from Experimental Transport Behaviour of Molten Salts and Structural Properties. *Z. Naturforsch.* **1976**, *31*, 967-973.
- (57) Zwanzig, R. On the relation between self-diffusion and viscosity of liquids. *J. Chem. Phys.* **1983**, *79*, 4507-4508.
- (58) Brillo, J.; Pommrich, A. I., Meyer, A. Relation between Self-Diffusion and Viscosity in Dense Liquids: New Experimental Results from Electrostatic Levitation. *Phys. Rev. Lett.* **2011**, *107*, 165902.
- (59) Ni, H.; Wu, J.; Sun, Z.; Lu, G.; Yu, J. Insight into the viscosity enhancement ability of $\text{Ca}(\text{NO}_3)_2$ on the binary molten nitrate salt: A molecular dynamics simulation study. *Chem. Eng. J.* **2019**, in press. DOI: 10.1016/j.cej.2018.09.190
- (60) Molinder, R.; Comyn, T. P.; Hondow, N.; Parker, J. E.; Dupont, V. In situ X-ray diffraction of CaO based CO_2 sorbents. *Energy Environ. Sci.* **2012**, *5*, 8958-8969.

Graphical TOC

